NATIONAL AERONAUTICS AND SPACE ADMINISTRATION

TECHNICAL MEMORANDUM X-787

A WIND-TUNNEL INVESTIGATION OF THE DYNAMIC STABILITY OF AXISYMMETRIC MODELS WITH HAMMERHEAD NOSES IN TRANSONIC FLOW*

By Robert C. Robinson

SUMMARY

The dynamic characteristics of six axisymmetric hammerhead models have been investigated at transonic Mach numbers by both forced- and free-oscillation techniques. The tests covered a range of Mach numbers from 0.70 to 1.20 at Reynolds numbers from 2.4×10^6 to 2.8×10^6 based on the reference diameter. Damping data are presented for a mean angle of attack of 0° and free-oscillation data for angles of attack of 0°, 2°, and 4°. Schlieren motion pictures of the flow during free-oscillation tests are available in a film supplement. It was found that the configurations with boattail angles of 10° and 20° were dynamically unstable at some Mach numbers for a mean angle of attack of 0°.

INTRODUCTION

In order to avoid excessive structural weight for space vehicles, knowledge of the loads to which they will be subjected is of critical importance to the designer. One area of uncertainty is the aerodynamic loading encountered at transonic Mach numbers during launch. This is particularly true of the dynamic loads on hammerhead configurations, those with payload packages which are larger in diameter than upper stage rockets. A research program was undertaken at Ames Research Center to investigate these dynamic loads through measurements of fluctuating pressures on rigid models and the damping characteristics of dynamic models. The data presented in references 1 and 2 show the presence of regions of large pressure fluctuations associated with shock wave motion and with flow separation over converging sections of launch configurations. In reference 3, it is shown that the structural response to the pressure fluctuations may be greatly influenced by aerodynamic damping derivatives. In the present report, aerodynamic damping is investigated for six hammerhead configurations in order to show some of the effects of nose shape and boattail angle. Results are given in terms of aerodynamic damping derivatives and root-mean-square bending moments obtained from forced-oscillation and free-oscillation tests, respectively.

Motion picture supplement 111 has been prepared and is available on loan. A request card and a description of the film are included at the back of this document.

*Title, Unclassified

[redacted]

NOTATION

C_m pitching-moment coefficient, $\frac{\text{pitching moment}}{\frac{1}{2}\rho_\infty V_\infty^2 Sd}$

d diameter of aft cylindrical portion of model, ft

k reduced frequency parameter, $\frac{\omega d}{V_\infty}$

q angular velocity due to pitching, radians/sec

S $\frac{\pi d^2}{4}$, sq ft

V_∞ free-stream velocity, ft/sec

α mean angle of attack, deg

α_o oscillation amplitude (one half of peak-to-peak value), deg

$\dot{\alpha}$ time rate of change of angle of attack, radians/sec

ρ_∞ mass density of air in the free stream, slugs/cu ft

ω angular frequency of oscillation, radians/sec

When $\dot{\alpha}$ and q are used as subscripts, a dimensionless derivative is indicated.

$$C_{m_q} + C_{m_{\dot{\alpha}}} = \left[\frac{\partial C_m}{\partial(qd/V_\infty)}\right] + \left[\frac{\partial C_m}{\partial(\dot{\alpha}d/V_\infty)}\right]$$

APPARATUS AND INSTRUMENTATION

Models

Six axisymmetric models were used in these tests. The model numbers 7(b), 8(a), 11(b), 22, 23, and 24 were assigned to the six models as part of the overall Ames Research Center test program numbering system. Figure 1(a) is a sketch of model 8(a) with the 15° nose of model 24 shown by dashed lines. Models 11(b), 22, and 23 differed from each other only in boattail angle and length of the aft cylindrical section as shown in figure 1(b). Figure 1(c) is a sketch of model 7(b).

It was necessary to keep the weight of the models to a minimum in order to obtain the oscillation frequencies desired for the tests, but it was also necessary to have a high degree of model rigidity to maintain one-degree-of-freedom motion. This was accomplished by using a sandwich type of construction in building the models. The inner and outer skins were thin glass-cloth laminates

separated by a half-inch layer of a foamed material having a density of 2 pounds per cubic foot. A short aluminum cylinder was glued to the inner skin of each model to provide a means of attachment to the balances.

Wind Tunnel

All the tests reported herein were conducted in the Ames 14-Foot Transonic Wind Tunnel which has a perforated test section that permits testing at and near the speed of sound. The tunnel is operated at a constant stagnation pressure approximately equal to atmospheric pressure. An air exchanger is used to control the tunnel stagnation temperature between limits of 60° and 180° F. The model support system consists of a sting mounted on a large strut which spans the tunnel downstream of the test section. For some of the tests, in order to put the model frequency between sting natural frequencies, a 2000 pound weight was suspended from the sting by a strut to lower the sting first bending frequency to approximately 3 cycles per second. Figure 2 shows model 8(a) mounted in the wind tunnel.

Balances

The balance for the forced-oscillation tests was a hydraulic servo oscillator which drove the models in a one-degree-of-freedom pitching motion. A drawing of the balance is shown in figure 3, and figure 4 is a photograph of the balance. The axis of rotation is fixed by crossed flexures. Resonant frequency of the complete system is a function of the model moment of inertia and the total spring constant, which is the sum of the restoring moments due to resonance springs and the crossed flexures and to the aerodynamic restoring moment.

A block diagram of the instrumentation is shown in figure 5. Two strain gages on the resonance springs and two on the torque arm were used to measure components of the model position and of the driving torque in phase with position and velocity. Power amplifiers, driven by a variable-frequency two-phase oscillator, powered the in-phase (with position) gages with a sine signal and the out-of-phase gages with a cosine signal. The sine signal was also used to drive the servo amplifier after passing through a phase-shift network which could be adjusted to compensate for phase shifts in the servo system and thus maintain the model motion in phase with the sine signal. The outputs of the in-phase and out-of-phase gages (which are the product of the powering signals and the stress in the gages) contained steady components proportional to the peak magnitude of the model position or the driving torque. After time-varying components were removed by filtering, the steady components were converted to digital form and used in computing $C_{m_q} + C_{m_{\dot{\alpha}}}$. The principle of multiplying the powering signal and the gage stress to obtain a steady output proportional to the peak load is discussed in more detail in reference 4.

For the free-oscillation tests, the models were mounted on a short cantilever spring which fixed the axis of rotation of the model at the same position as

for the forced-oscillation tests. A sketch of the spring and model mounting plate is shown in figure 6. The spring was instrumented with strain gages calibrated to measure model angle of attack and spring restoring moment. Magnetic tape was used to record the output of the gages which was proportional to the bending moment acting on the model in the pitch plane, and from those records the root mean squares of bending moment and of model oscillation amplitude were computed. The instrumentation used in recording the data and measuring the root-mean-square values was the same as that described in reference 1.

TESTS AND PRECISION

Forced-Oscillation Tests

Models and test conditions.- Forced-oscillation tests were made with models 7(b), 8(a), 11(b), 23, and 24. The models were oscillated about an axis of rotation located in the base plane of the model. Aft of the axis of rotation, the sting was shrouded by a fairing with the same diameter as the base of the model. With this arrangement, the one-degree-of-freedom motion of the model provided an approximate simulation of the motion of the nose of a bending vehicle.

The models were oscillated about zero angle of attack at peak amplitudes of $1/4^{\circ}$ and $1/2^{\circ}$ at frequencies of 7 to 20 cycles per second. The corresponding range of reduced frequency parameter k was from 0.03 to 0.09. The Mach number range for the tests was from 0.70 to 1.10 while Reynolds number, referenced to base diameter, varied from 2.4 to 2.8 million, depending on Mach number and wind-tunnel stagnation temperature.

Precision and corrections.- Dynamic calibrations of the balance and associated electronic equipment have shown that steady damping moments can be measured within ±2 percent. However, when models are dynamically stable and aerodynamic damping moments are being measured at transonic Mach numbers, the uncertainty is believed to increase to about ±5 percent. When the models were dynamically unstable, the damping measurements fluctuated as much as ±50 percent and the data presented for such conditions were computed from the average of three readings taken near the middle value of the damping fluctuations.

The amplitude of oscillation was measured with an accuracy of $\pm 0.02^{\circ}$ and the frequency with an accuracy of ±0.01 cycle per second. The free-stream Mach number was accurate to ±0.002 and the mean angle of attack to $\pm 0.1^{\circ}$.

Damping tares obtained from wind-off tests were used to correct the data for structural damping of the balance and for still air damping. The structural damping of the models was negligible. No corrections were made for tunnel-wall interference or air-stream angle.

Free-Oscillation Tests

Models and test conditions.- Models tested in free oscillation were 7(b), 11(b), 22, 23, and 24. The Mach number range of the tests was from 0.70 to 1.20 and the Reynolds number range was from 2.4 to 2.8 million, but data could not be taken at conditions where the motion was divergent. Tests were made at nominal angles of attack of 0°, 2°, and 4°. As in the case of the forced-oscillation tests, the axis of rotation was in the plane of the model base. Structural damping in the model mode, computed from decay records, varied from about 1/2 of 1 percent to 3 percent of critical. The sting modes also were variable because of changes in the restraint between tests. Peak amplitudes varied from less than 0.1° to about 1°, depending on buffeting level and aerodynamic damping. The wind-off resonant frequencies of the models were between 20 and 24 cycles per second. Schlieren motion pictures at 64 frames per second were taken during the free-oscillation tests and are presented in a film supplement.

Precision.- In the free-oscillation tests, the Mach number was set to within ±0.01. The nominal angle of attack could be set within ±0.1° but static deflection, due to lift loads, caused the true mean angle of attack to be larger than the nominal 2° or 4° by 5 to 20 percent, depending on the model and the Mach number.

The effect of static loads was eliminated from the root-mean-square bending moment by a high pass filter in the tape record circuit and a band pass filter in the root-mean-square recording circuit. The filter characteristics are shown in reference 2. The rms data presented are the average of 20 digital readings distributed over the duration of the 1-minute record taken for each data point.

RESULTS AND DISCUSSION

Forced-Oscillation Tests

The results of the forced-oscillation tests of models 7(b), 8(a), 11(b), 23, and 24 are presented in figure 7 in which the damping-in-pitch coefficient $C_{m_q} + C_{m_{\dot{\alpha}}}$ is plotted as a function of Mach number for a mean angle of attack of 0°. When aerodynamic damping is destabilizing, $C_{m_q} + C_{m_{\dot{\alpha}}}$ is positive. Figure 7(a) shows that model 8(a) was dynamically unstable over a Mach number range from about 0.80 to nearly 1.00 with the maximum $C_{m_q} + C_{m_{\dot{\alpha}}}$ of 130 occurring at $0.90 < M < 0.93$. The variation of $C_{m_q} + C_{m_{\dot{\alpha}}}$ with Mach number was smooth and the effect of amplitude was small.

Changing the nose angle from 30° to 15° resulted in a very different variation of $C_{m_q} + C_{m_{\dot{\alpha}}}$ with Mach number as may be seen in figure 7(b). At $0.90 < M < 0.93$, where model 8(a) (30° nose) was most unstable, model 24 (15° nose) was slightly stable with regions of instability at higher and lower Mach numbers. The lower unstable region is broad with a $C_{m_q} + C_{m_{\dot{\alpha}}}$ of approximately

[redacted]

50 at $M \approx 0.80$, while the upper region is narrow with the damping-in-pitch coefficient reaching 550 for $\alpha_o = 1/4^o$ at $M \approx 0.95$. The dashed fairing where forced-oscillation data were not taken is based on observations of the model behavior during the free-oscillation tests.

A further change in nose shape, to that of model 23 with the 10° boattail somewhat closer to the pivot point, resulted in a small stable shift of the entire $C_{m_q} + C_{m_{\dot{\alpha}}}$ curve. This is shown in figure 7(c). Considering the limitations of accuracy for damping readings, model 23 was essentially neutral in stability at $M = 0.70$ and 0.80. The narrow region of instability near $M = 0.95$ was still present but reduced in intensity by about 50 percent compared to model 24.

Damping data for model 11(b) presented in figure 7(d) show that the 34° boattail angle resulted in a dynamically stable configuration for the Mach numbers and amplitudes covered in these tests. It should be noted that unlike the preceding three models, model 11(b) was measurably less stable at an amplitude of $1/2^o$ than at $1/4^o$.

Tests of model 8(a) provided an additional indication of the effect of boattail angle on the dynamic stability of hammerhead configurations. As may be observed in figure 7(e), model 8(a), with its 6-$1/2^o$ boattail, was stable for an amplitude of $1/2^o$ and, while the stability decreased for the $1/4^o$ amplitude, the model did not become significantly unstable for the test conditions.

Free-Oscillation Tests

Results from the free-oscillation tests are presented to show the effect of angle of attack on the dynamic stability of hammerhead configurations. Quantitative comparisons of rms between models cannot be made without taking structural damping and sting mode effects into account, but the effect of angle of attack on the separate models can be determined. Typical time histories of model dynamic response are shown in figure 8, and in figure 9 the root mean square of bending moment in the model support spring is plotted against Mach number for models 24, 11(b), 22, 23, and 7(b).

When the models were tested on the free-oscillation apparatus, the response of the model-spring systems varied from a random-pulse type to divergence depending on the combined aerodynamic and mechanical damping. The random-pulse type of response shown in figure 8(a) was observed under conditions of high net damping. Under conditions of low net damping, the models responded in random bursts of divergent-convergent oscillations at the resonant frequency of the model-spring system as shown in figure 8(b). The record of an oscillation at nearly constant amplitude presented in figure 8(c) was obtained from model 24 (15° nose with 10° boattail) at $M = 0.80$ and $\alpha = 0^o$ where the measured value of $C_{m_q} + C_{m_{\dot{\alpha}}}$ was approximately 50 for an amplitude of $1/2^o$, which should result in divergent oscillation for the system. The limit amplitude of approximately 0.8^o was probably due to a decrease in $C_{m_q} + C_{m_{\dot{\alpha}}}$ with increasing amplitude. A time history

in a region of divergence, shown in figure 8(d), was obtained by decreasing Mach number rapidly from $M = 1.00$ with model 23 at zero angle of attack. When the flow Mach number reached the narrow unstable range at $M = 0.95$, a divergent oscillation began to develop but was damped quickly as the Mach number dropped below the critical value.

Free-oscillation data presented for model 24 in figure 9(a) show that, while the response of the model at $\alpha = 0^\circ$ corresponded to the measured values of damping shown in figure 7(b), the instability at Mach numbers of 0.80 and 0.95 for $\alpha = 0^\circ$ did not appear at angles of attack of 2° and 4°. With the exception of $\alpha = 0^\circ$, the rms bending moment in the model supporting spring varies from a low value of 100 in-lb at $M = 0.70$ to a maximum of about 1000 in-lb at $M = 0.90$ and then down to 125 in-lb at $M = 1.00$. Data points for $\alpha = 0^\circ$ fall on the same curve except at Mach numbers of 0.80 and 0.95 where measured aerodynamic damping was of opposite sign and greater magnitude than the structural damping. At $M = 0.80$ and $\alpha = 0^\circ$ (part of this record is shown in fig. 8(c)), an rms of 1400 in-lb was measured but it was not possible to obtain data at $M = 0.95$ and $\alpha = 0^\circ$ as the response of the model would have exceeded the allowable deflection of the support spring.

The data in figure 9(a) indicate that model 24 is unstable only at mean angles of attack at or near 0°. Except for the Mach numbers where instability occurred, angle of attack had little effect on the response of this model.

The motion of model 23 was also divergent at $\alpha = 0^\circ$ and $M = 0.95$, as would be expected from the damping measurements. The dynamic response data in figure 9(b) show that, as for the conical-nosed models, the dynamic instability occurred only for mean angles of attack at or near 0°.

Dynamic response data for models 22, 11(b), and 7(b) are presented for Mach numbers up to 1.00 in figures 9(c), 9(d), and 9(e), respectively. The variation of the response of these models with Mach number was small compared to that of the models having 10° boattails.

Additional free-oscillation tests were made of model 22 (20° boattail) at Mach numbers up to 1.20 because it was considered possible that increasing the boattail angle would cause dynamic instability to occur at higher Mach numbers. It was found that this model did develop a divergent oscillation at $M = 1.20$. Although a time history from the strain gage was not recorded, motion pictures at 64 frames per second were obtained of a sustained oscillation which developed at this Mach number. Model deflections were measured from the film and plotted against time in figure 10. The points were then fitted with exponential sine waves by the method of reference 5. The divergent oscillation on the figure indicates that aerodynamic damping was destabilizing.

CONCLUDING REMARKS

Free- and forced-oscillation tests of six hammerhead configurations show that such configurations can lead to dynamic instability at transonic Mach numbers. The dynamic response of the free-oscillation models indicated that the instability occurred only at angles of attack near zero.

Within the limits of these tests, with the center of rotation at the base of the model, it appears that boattail angle has more influence on dynamic stability than does nose shape. Three models with 10° boattails were unstable subsonically and one with a 20° boattail was unstable at $M = 1.20$. No instability was found for a model with a 34° boattail while one with a $6\text{-}1/2^\circ$ boattail was marginally stable for some test conditions.

Ames Research Center
National Aeronautics and Space Administration
Moffett Field, Calif., Dec. 27, 1962

REFERENCES

1. Coe, Charles F.: Steady and Fluctuating Pressures at Transonic Speeds on Two Space-Vehicle Payload Shapes. NASA TM X-503, 1961.

2. Coe, Charles F., and Nute, James B.: Steady and Fluctuating Pressures at Transonic Speeds on Hammerhead Launch Vehicles. NASA TM X-778, 1962.

3. Cole, Henry A., and Coe, Charles F.: Dynamic Response of Hammerhead Launch Vehicles to Transonic Buffeting. Paper for Seventh Symposium on Ballistic Missile and Space Technology, Aug. 1962.

4. Reese, David E., Jr.: An Experimental Investigation of the Unsteady Lift Induced on a Wing in the Downwash Field of an Oscillating Canard Control Surface. NACA RM A55F01, 1955.

5. Ellington, J. P., and McCallion, H.: The Analysis of Transient Vibration Data. Jour. Roy. Aero. Soc., vol. 60, no. 550, Oct. 1956, pp. 679-680.

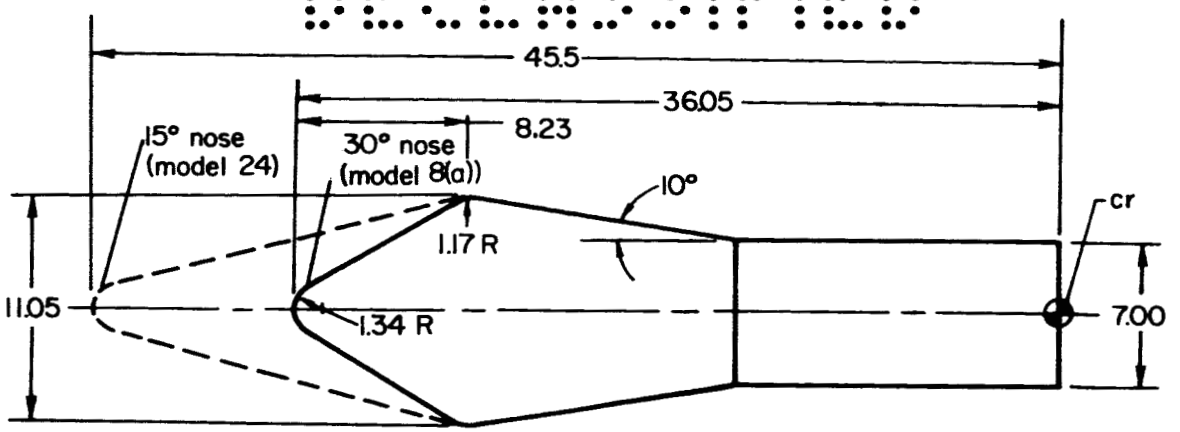

(a) Models 8(a) and 24.

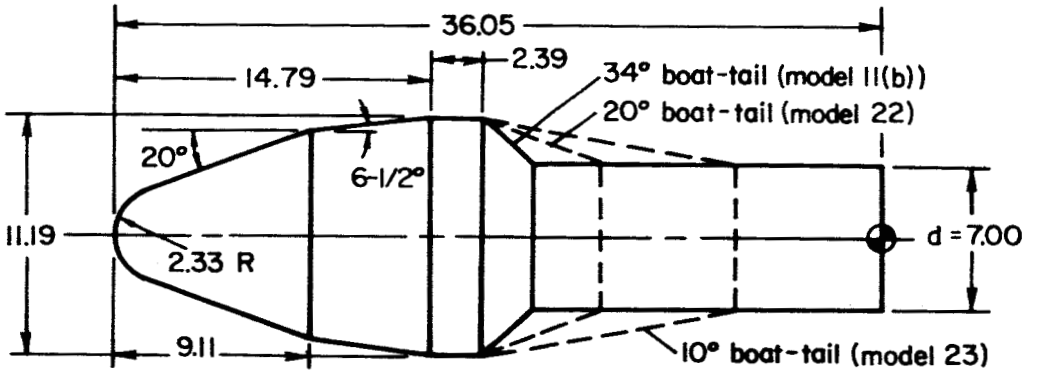

(b) Models 11(b), 22, and 23.

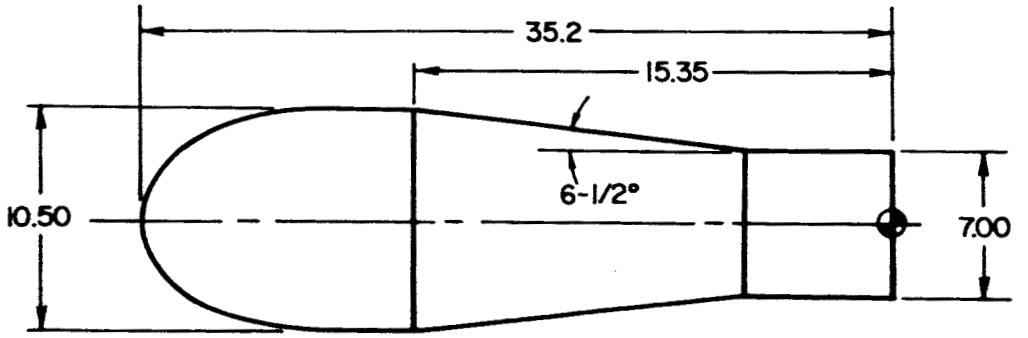

Note: All dimensions in inches.

(c) Model 7(b).

Figure 1.- Sketches of models.

[redacted]

A-28133

Figure 2.- Model 8(a) in the wind tunnel.

[redacted]

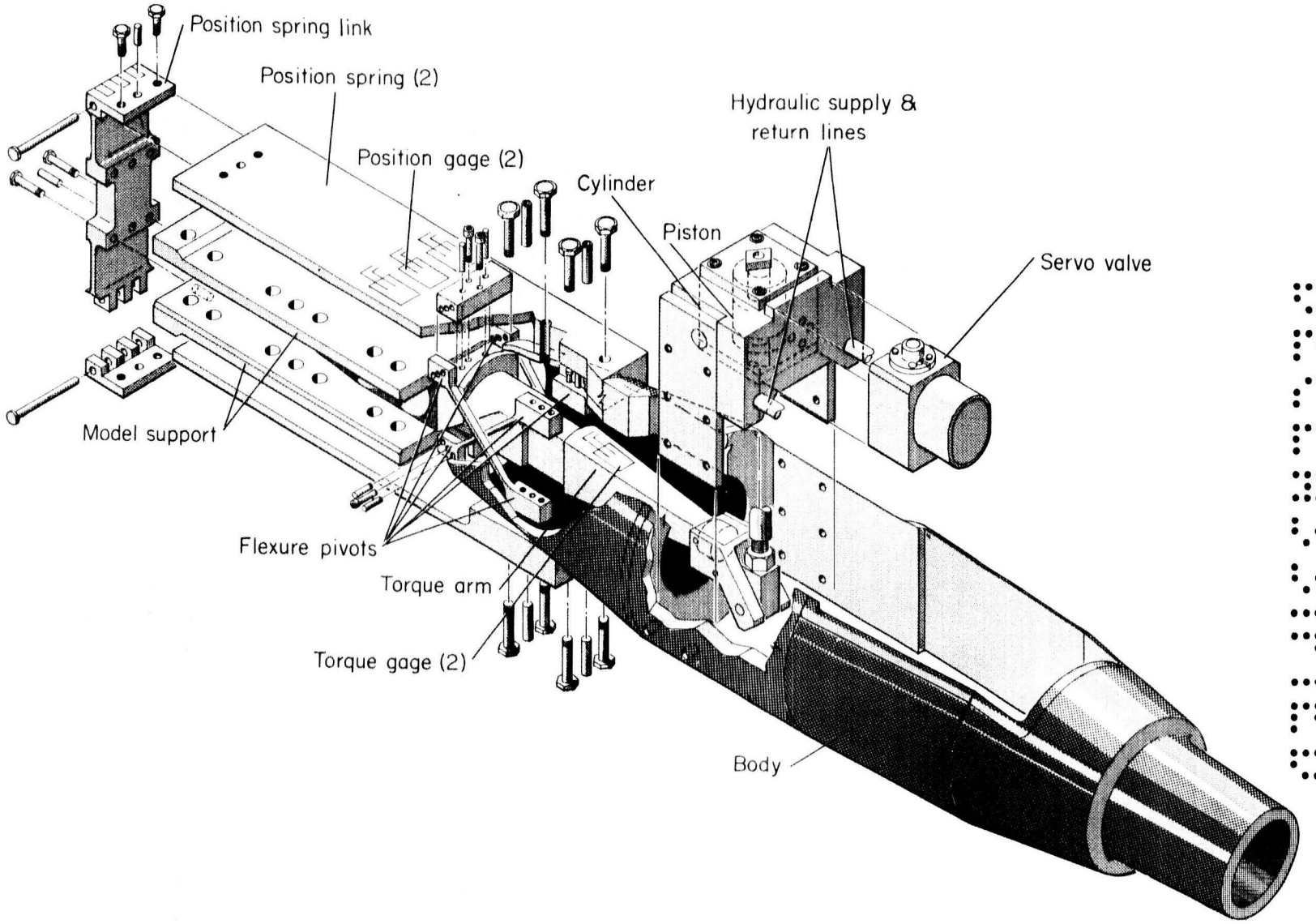

A-26017-1

Figure 3.- Drawing of the forced-oscillation balance.

Figure 4.- Photograph of the forced-oscillation balance.

A-25200

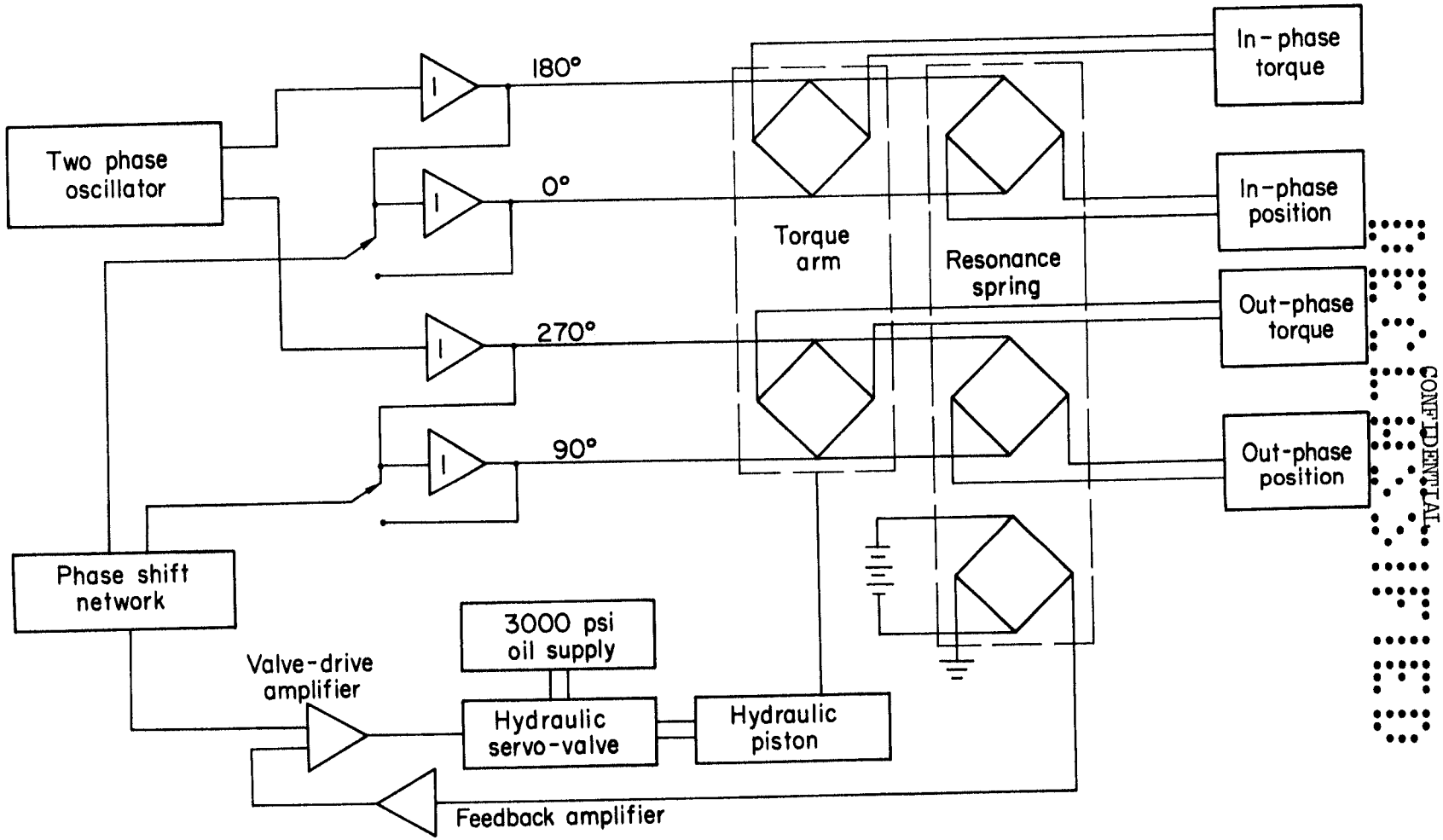

Figure 5.- Block diagram of the instrumentation for the forced-oscillation tests.

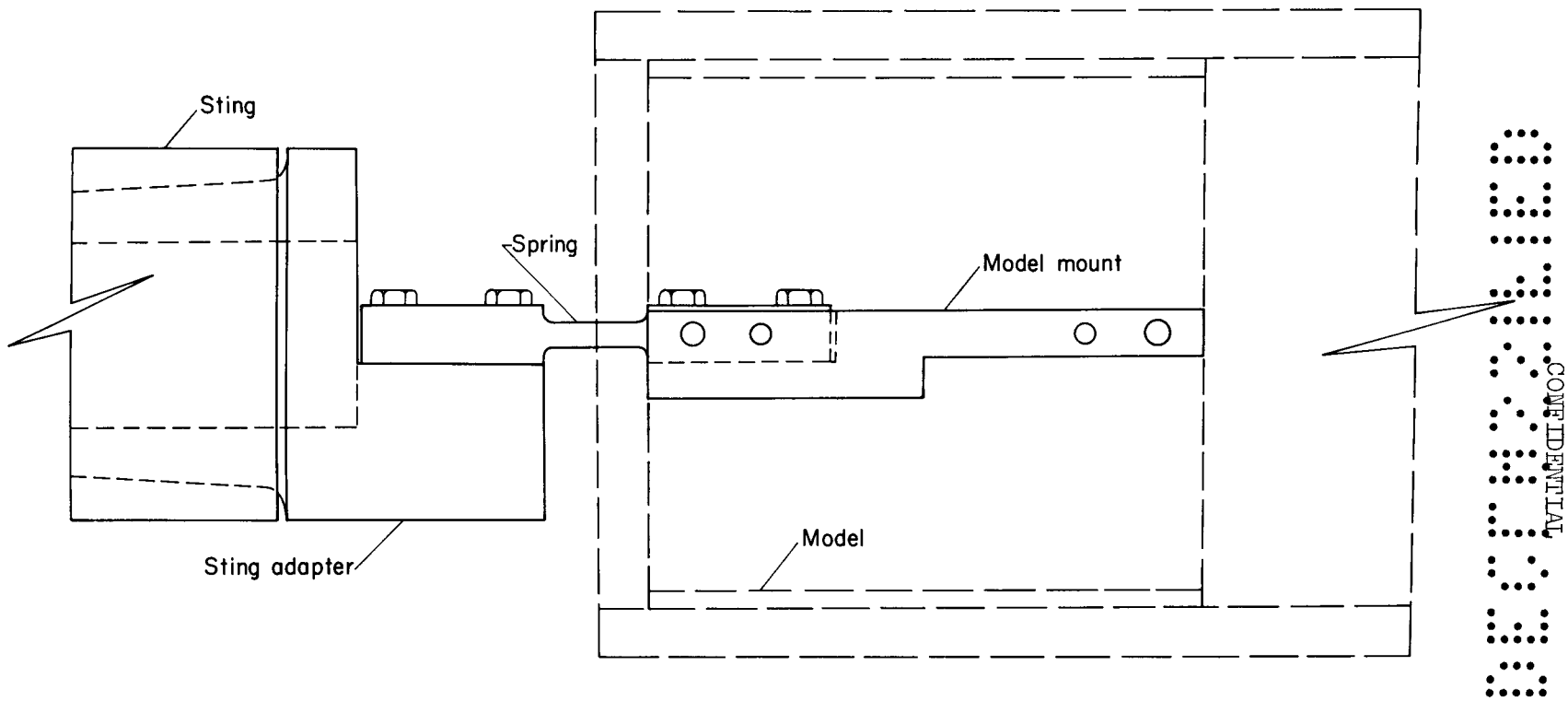

Figure 6.- Sketch of the free-oscillation balance.

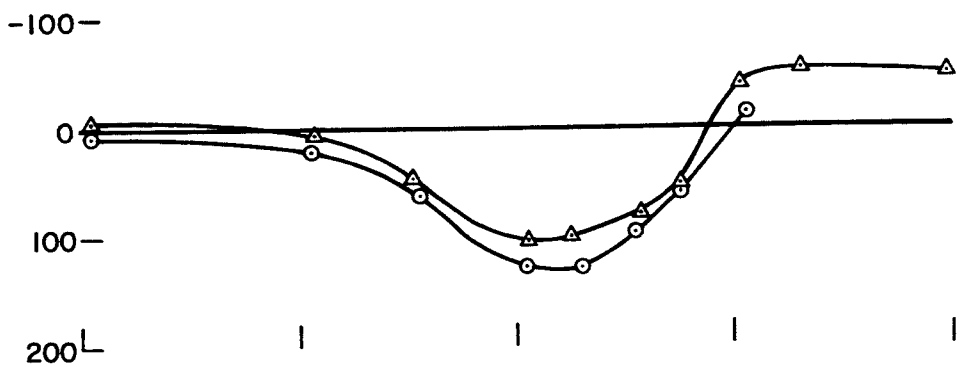

(a) Model 8(a) (30° nose).

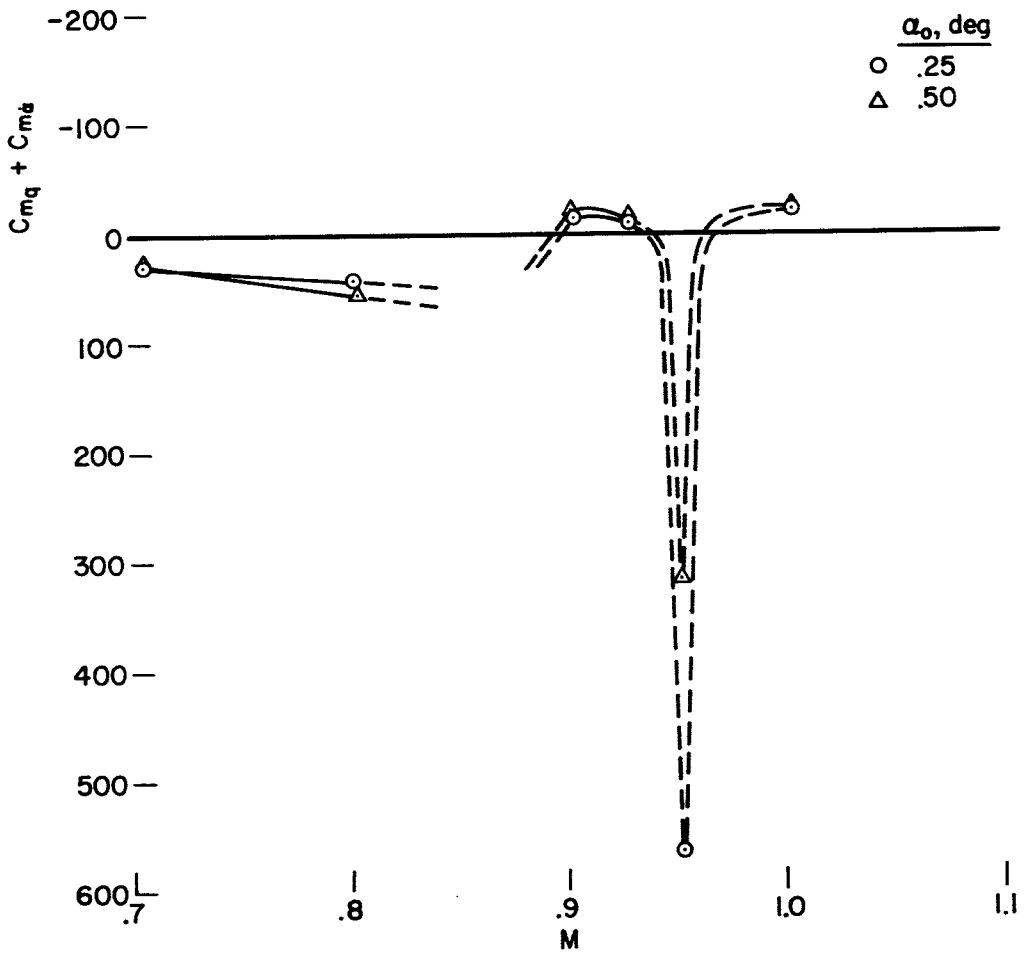

(b) Model 24 (15° nose).

Figure 7.- The variation of the damping-in-pitch parameter with Mach number for a mean angle of attack of 0°, from forced-oscillation tests.

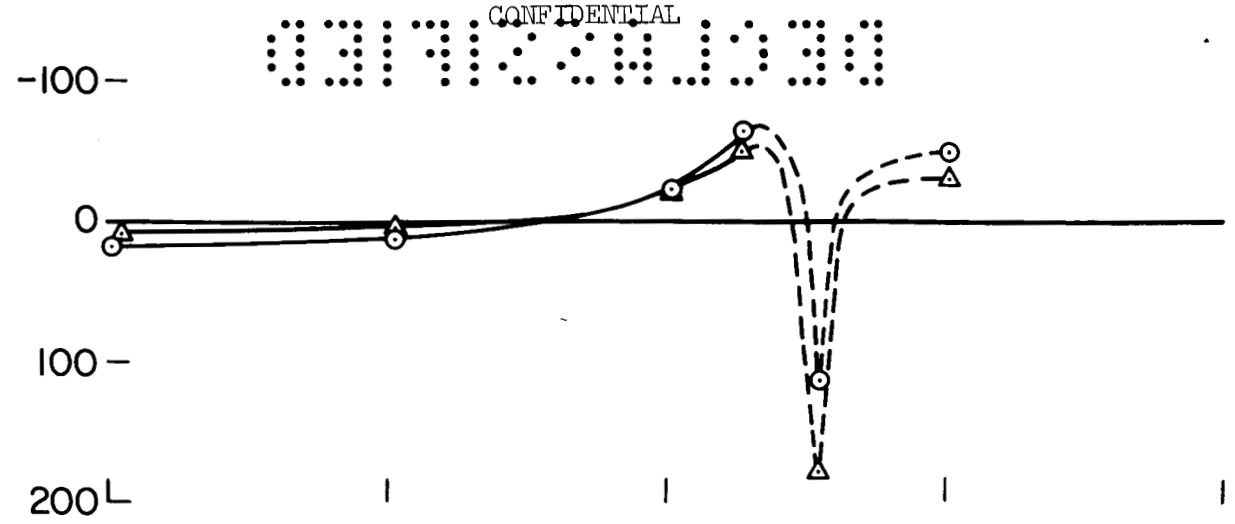

(c) Model 23 (10° boattail).

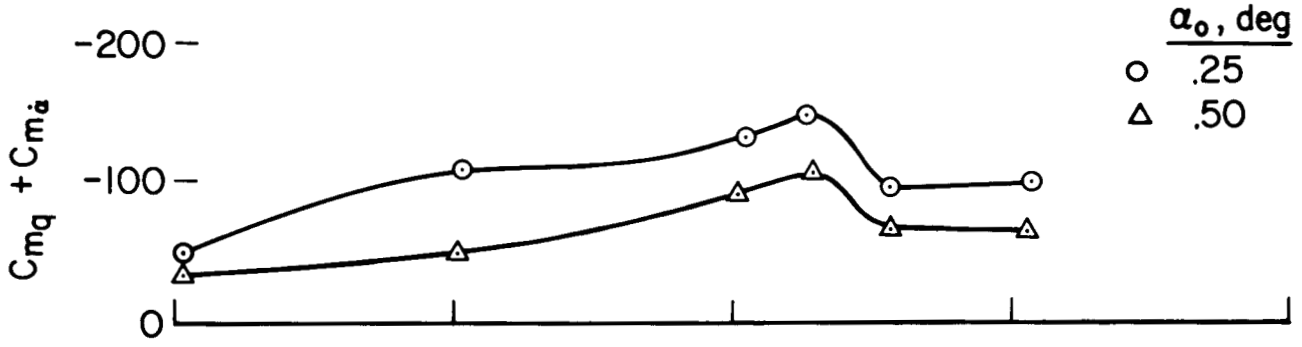

(d) Model 11(b) (34° boattail).

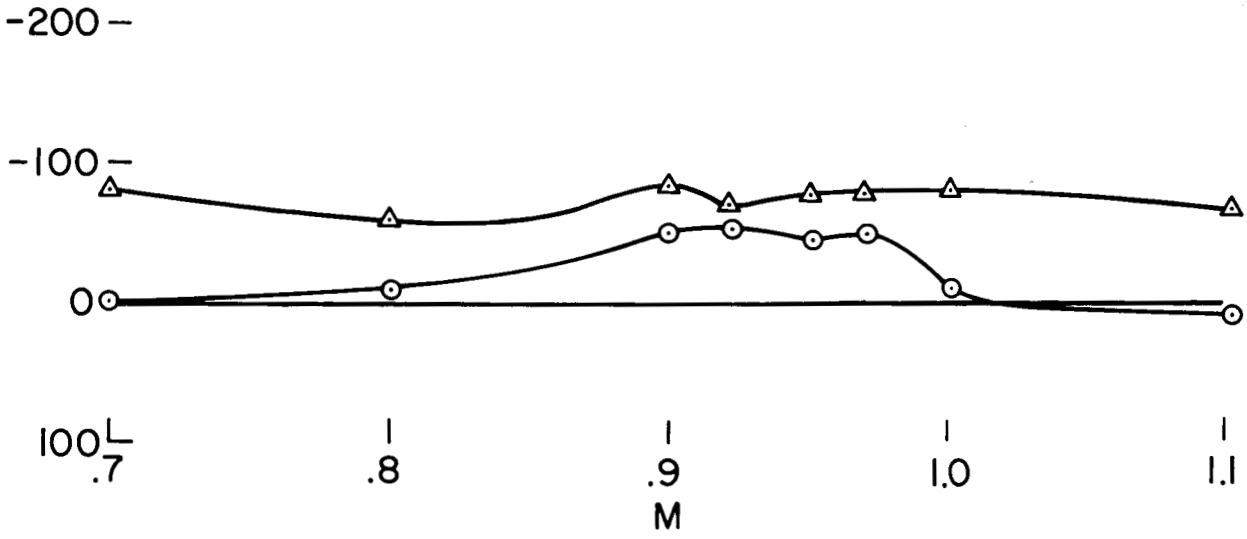

(e) Model 7(b).

Figure 7.- Concluded.

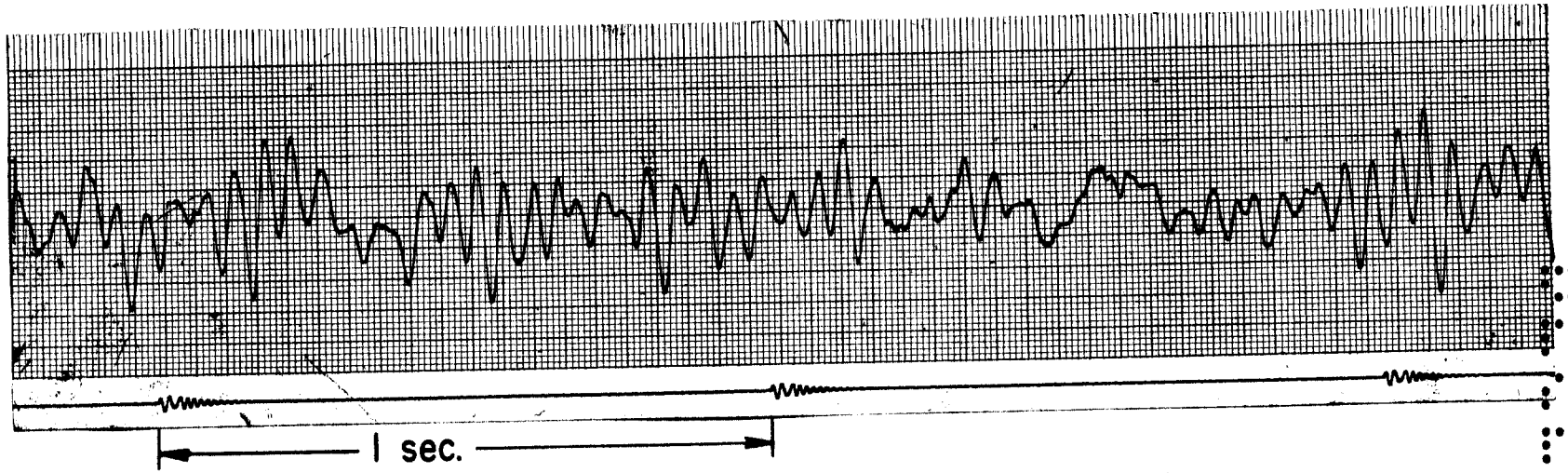

(a) High net damping, model 11(b), M = 0.95, $\alpha = 0^{o}$.

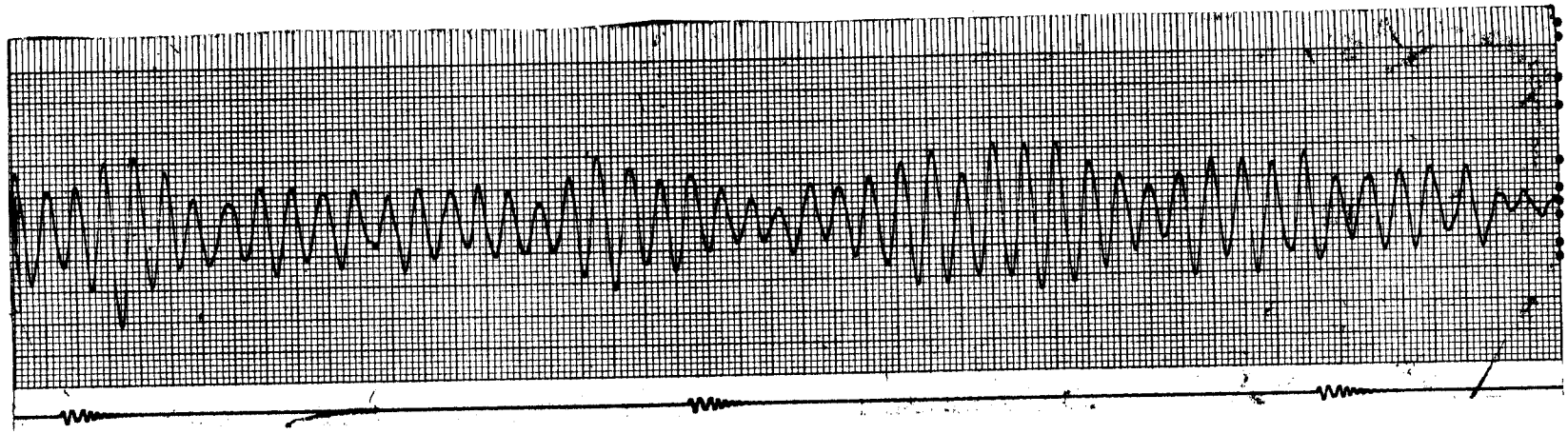

(b) Low net damping, model 24, M = 0.90, $\alpha = 0^{o}$.

Figure 8.- Typical time histories of model angular response in free oscillation for various damping conditions.

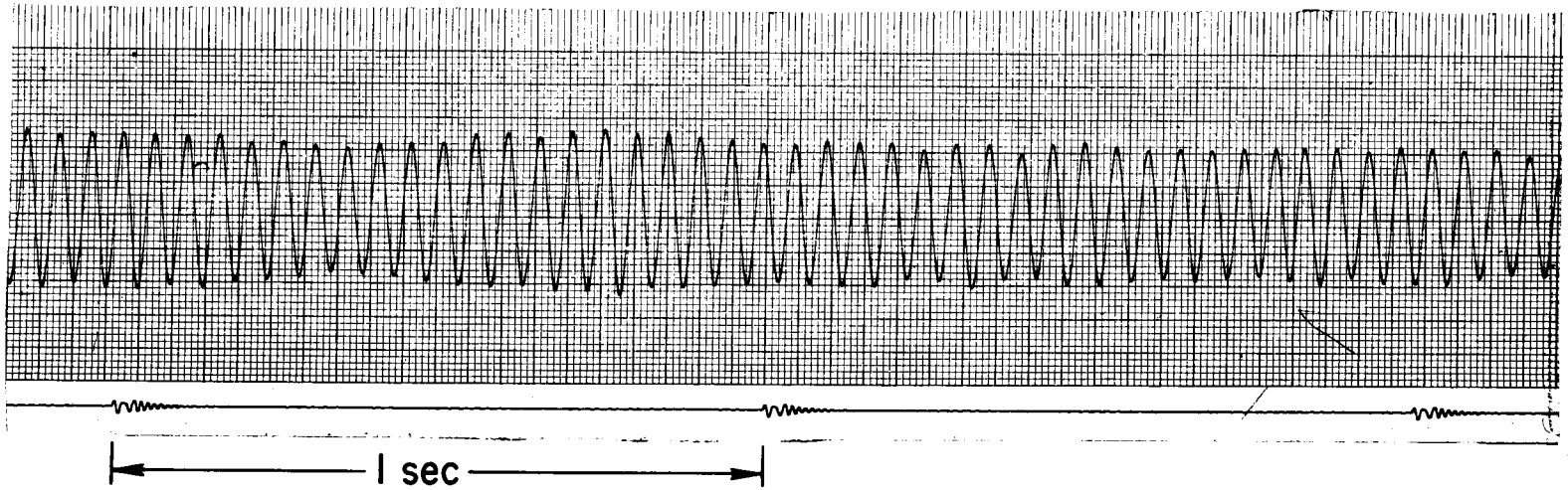

(c) Net damping of zero, model 24, M = 0.80, $\alpha = 0^{\circ}$.

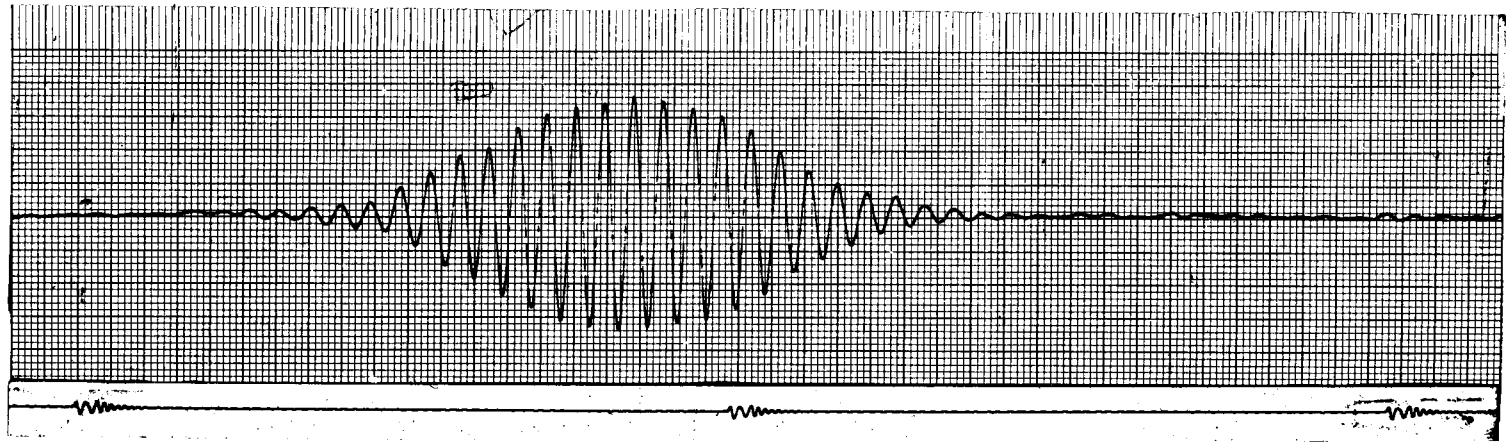

(d) Negative net damping, model 23, M = 1.00 → 0.90, $\alpha = 0^{\circ}$.

Figure 8.- Concluded.

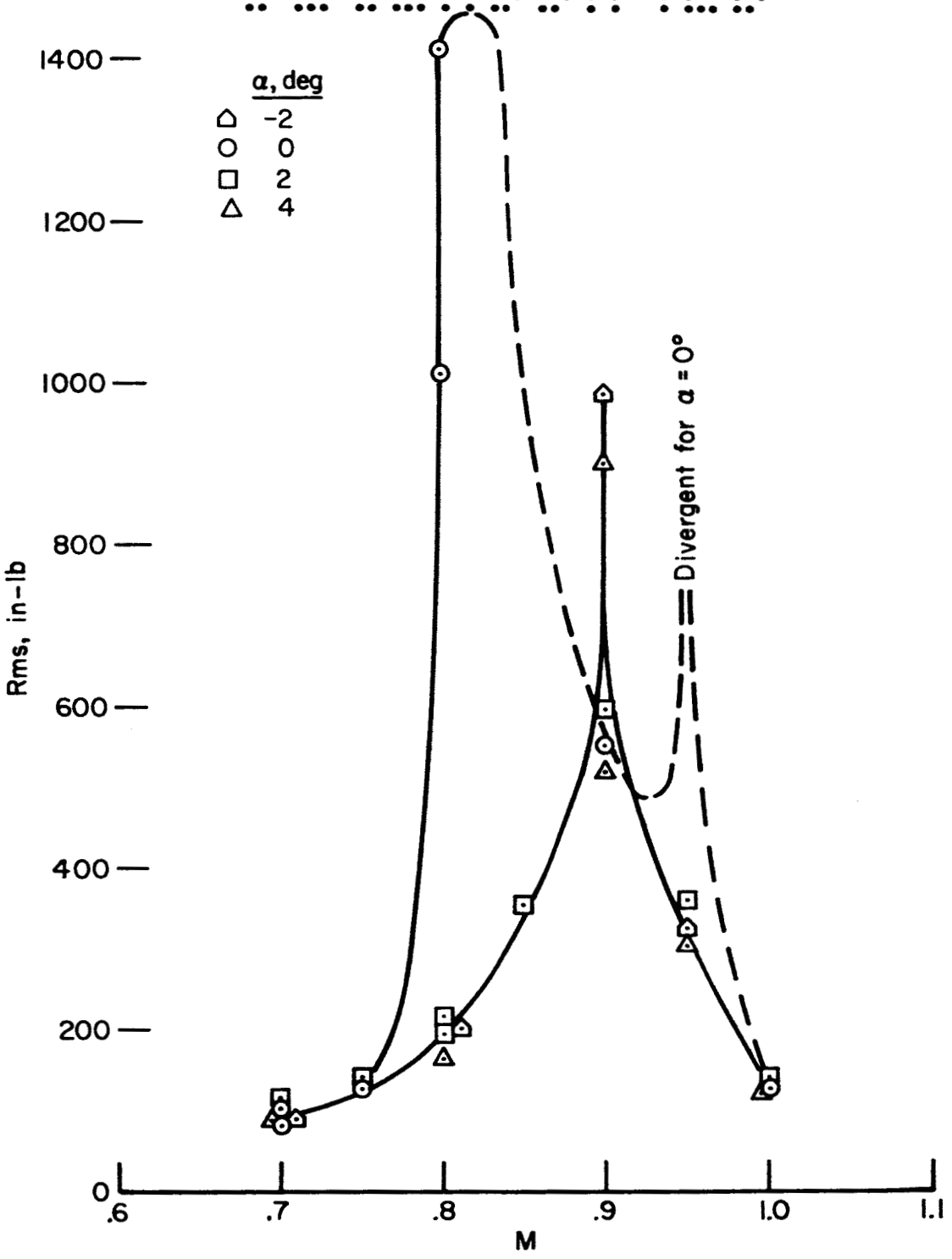

(a) Model 24 (15° nose, 10° boattail).

Figure 9.- Variation with Mach number of the root mean square of bending moment in the model support spring, from free-oscillation tests.

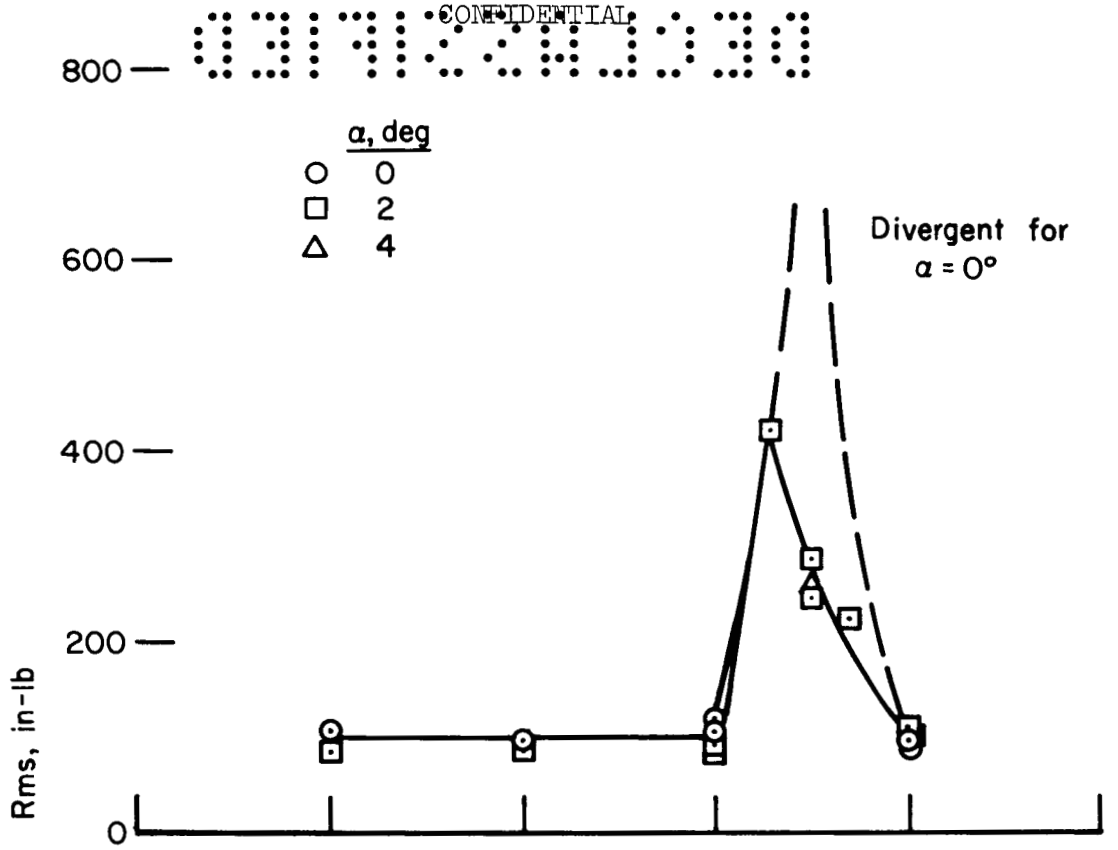

(b) Model 23 (10° boattail).

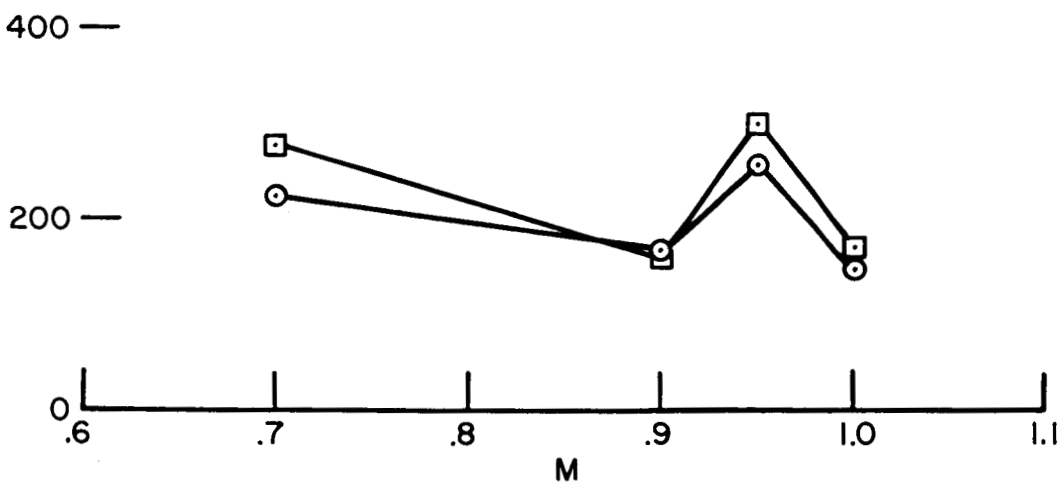

(c) Model 22 (20° boattail)

Figure 9.- Continued.

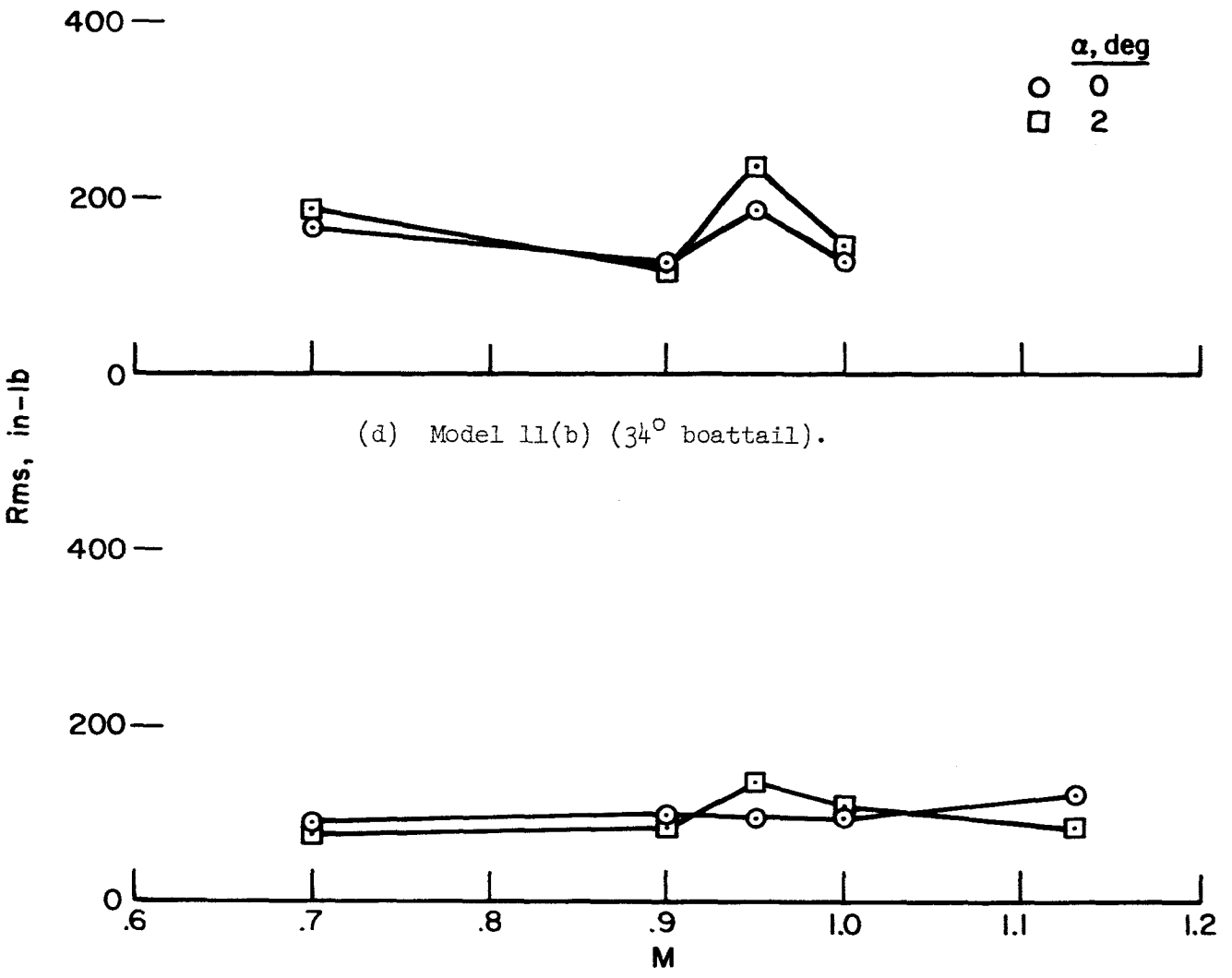

(d) Model 11(b) (34° boattail).

(e) Model 7(b).

Figure 9.- Concluded.

Figure 10.- Augular response of model 22 (20° boattail) at M = 1.20 and $\alpha = 0°$.

NASA-Langley, 1963 A-623